Tellus
SERIES A
DYNAMIC
METEOROLOGY
AND OCEANOGRAPHY
PUBLISHED BY THE INTERNATIONAL METEOROLOGICAL INSTITUTE IN STOCKHOLM

Tellus (2008), 60A, 946–961
Printed in Singapore. All rights reserved

TELLUS

Comparison of equilibrium and transient responses to CO_2 increase in eight state-of-the-art climate models

By TOKUTA YOKOHATA[1]*, SEITA EMORI[1,2,4], TORU NOZAWA[1], TOMOO OGURA[1], MICHIO KAWAMIYA[2], YOKO TSUSHIMA[2], TATSUO SUZUKI[2], SEIJI YUKIMOTO[3], AYAKO ABE-OUCHI[2,4], HIROYASU HASUMI[4], AKIMASA SUMI[5] and MASAHIDE KIMOTO[4], [1]*National Institute for Environmental Studies, Tsukuba, Japan;* [2]*Frontier Research Center for Global Change, Yokohama, Japan;* [3]*Meteorological Research Institute, Tsukuba, Japan;* [4]*Center for Climate System Research, University of Tokyo, Kashiwa, Japan;* [5]*Transdisciplinary Initiative for Global Sustainability, Tokyo, Japan*

(Manuscript received 10 October 2007; in final form 3 June 2008)

ABSTRACT

We compared the climate response of doubled CO_2 equilibrium experiments ($2 \times CO_2$) by atmosphere–slab ocean coupled general circulation models (ASGCMs) and that of 1% per year CO_2 increase experiments ($1\%CO_2$ by atmosphere–ocean coupled general circulation models (AOGCMs) using eight state-of-the-art climate models. Climate feedback processes in $2 \times CO_2$ are different from those in $1\%CO_2$, and the equilibrium climate sensitivity ($T_{2\times}$) in $2 \times CO_2$ is different from the effective climate sensitivity ($T_{2\times,\mathrm{eff}}$) in $1\%CO_2$. The difference between $T_{2\times}$ and $T_{2\times,\mathrm{eff}}$ is from -1.3 to 1.6 K, a large part of which can be explained by the difference in the ice-albedo and cloud feedback. The largest contribution is cloud SW feedback, and the difference in cloud SW feedback for $2 \times CO_2$ and $1\%CO_2$ could be determined by the distribution of the SAT anomaly which causes differences in the atmospheric thermal structure. An important factor which determines the difference in ice-albedo feedback is the initial sea ice distribution at the Southern Ocean, which is generally overestimated in $2 \times CO_2$ as compared to $1\%CO_2$ and observation. Through the comparison of climate feedback processes in $2 \times CO_2$ and $1\%CO_2$, the possible behaviour of the time evolution of $T_{2\times,\mathrm{eff}}$ is discussed.

1. Introduction

Equilibrium climate sensitivity ($T_{2\times}$), defined as the globally and annually averaged surface air temperature (SAT) anomaly in the equilibrated states of atmospheric CO_2 doubling, is a measure of the equilibrium response to increased atmospheric CO_2 concentrations. The strength of climate feedback which determines $T_{2\times}$ is represented as a climate feedback parameter, $\lambda_{2\times}$, usually defined as the ratio of radiative forcing and $T_{2\times}$. $\lambda_{2\times}$ is used for simple energy balance climate models (Senior and Mitchell, 2000). The estimation by the climate models in the Intergovernmental Panel on Climate Change Fourth Assessment Report (IPCC AR4) is from 2.57 to 4.42 K, the range of which is calculated by using the average of 18 climate models and one standard deviation (Meehl et al., 2007b). In general, atmosphere–slab ocean coupled general circulation models (ASGCMs) are used for $T_{2\times}$ calculation in order to save integration time for the system to achieve equilibrium states. In ASGCMs, physical processes in the ocean are simplified and thus artificial heat flux is applied in the ocean-sea ice and held fixed under climate change conditions.

On the other hand, the transient climate response (TCR) to the gradual increase in greenhouse gases is more relevant if we consider near future time-dependent climate change. TCR can be calculated by atmosphere–ocean coupled general circulation models (AOGCMs), which include the physical processes in the ocean-sea ice system. The strength of the climate feedback in TCR is measured by 'effective climate sensitivity', $T_{2\times,\mathrm{eff}}$, which is defined as the equilibrium response to the doubling of atmospheric CO_2 if the climate feedback parameter is fixed to that diagnosed by the AOGCM run (Murphy, 1995).

In previous studies, it has been reported that $T_{2\times}$ is not equal to $T_{2\times,\mathrm{eff}}$. Senior and Mitchell (2000) reported that $T_{2\times} > T_{2\times,\mathrm{eff}}$ possibly because of the difference in the cloud response in the southern hemisphere. Kiehl et al. (2006) also reported $T_{2\times} > T_{2\times,\mathrm{eff}}$. On the other hand, Boer and Yu (2003) found the opposite, that is, $T_{2\times} < T_{2\times,\mathrm{eff}}$, due to the difference in tropical feedback. However, the details of the mechanisms which cause

* Corresponding author.
e-mail: yokohata.tokuta@nies.go.jp
DOI: 10.1111/j.1600-0870.2008.00345.x

the difference between in $T_{2\times}$ and $T_{2\times,\mathrm{eff}}$ have not been studied nor their model intercomparison has not been performed to date. Although statistical analyses of the relationship between $T_{2\times}$ and $T_{2\times,\mathrm{eff}}$ have been performed for some models (e.g. by Collins et al., 2006), the mechanism which causes their similarities and differences has not yet been investigated in detail. It is important to comprehend these mechanisms in order to understand how climate sensitivity depends on the climate states.

In this study, the differences in equilibrium and transient response to atmospheric CO_2 increase were investigated by using the results of the state-of-the art climate models from the World Climate Research Programme's (WCRP's) Coupled Model Intercomparison Project phase three (CMIP3) multimodel data set, which was referred to in the IPCC AR4 (Meehl et al., 2007a, hereafter 'CMIP3 climate models'). For this purpose, the climate feedback processes in the doubled CO_2 experiments ($2 \times CO_2$) by ASGCMs are compared to those in the 1% per year CO_2 increase experiments ($1\%CO_2$) by AOGCMs. Here, we also paid our attention to the difference in the numerical settings of ASGCMs and AOGCMs. The simplification of ocean processes adopted in ASGCMs may affect results in the equilibrium experiments.

The approximated partial radiative perturbation (APRP) method developed recently (Yokohata et al., 2005a,b; Taylor et al., 2007) was used for the climate feedback analysis. In the APRP method (Taylor et al., 2007), short-wave radiative feedback is accurately diagnosed by straightforward calculations using standard model outputs. In the conventional cloud radiative forcing (CRF) method, it has been reported that the non-cloud feedback component should be included in the cloud feedback (e.g. Colman, 2003; Soden et al., 2004). For example, Webb et al. (2006) investigated the cloud feedback analysis by the CRF method using various GCM ensembles, but some uncertainties remain at the high latitude region where the ice-albedo feedback is strong. In the APRP method, this problem does not occur because cloud feedback is clearly separated from ice-albedo feedback. Taylor et al. (2007) demonstrated that the short-wave feedback by the APRP method is a closer approximation of the more precise calculation of climate feedback called the perturbed radiative perturbation (PRP) method (e.g. Wetherald and Manabe, 1988). While several sophisticated techniques to diagnose climate feedback processes from model output have been proposed so far (e.g. Forster and Taylor, 2006; Winton, 2006), the APRP method is advantageous in that (1) it can diagnose both the cloud and ice-albedo feedback simultaneously and (2) it does not need additional off-line calculations such as those of the radiative kernel which are possibly dependent on the radiation model.

In Section 2, we present a description of the model data we used and give a brief explanation of the method of the climate feedback analysis. In Section 3, we describe the overall features of the climate feedback analysis (Section 3.1) and comparison of equilibrium and transient responses (Section 3.2), give a detailed explanation of ice-albedo feedback (Section 3.3) and cloud SW feedback (Section 3.4), with a focus on the differences between $2 \times CO_2$ and $1\%CO_2$ for each of the models. Finally in Section 4, we give a summary of our findings and discuss the results.

2. Model data and method of analysis

Climate feedback analysis was performed using the results of the $2 \times CO_2$ by ASGCM and $1\%CO_2$ by AOGCM of CMIP3 climate models (Table 1). We used the results of eight models which included both $2 \times CO_2$ and $1\%CO_2$ in the data archived by the Program for Climate Model Diagnosis and Intercomparison (PCMDI).

In $2 \times CO_2$, the monthly mean SAT and TOA radiative fluxes were taken from the last 20 yr, after the climate system reached equilibrium. Anomalies were calculated from the difference between the doubled CO_2 and control experiments. In $1\%CO_2$, the anomalies of SAT and TOA radiative fluxes were calculated

Table 1. Description of the CMIP3 climate models used for the climate feedback analysis

Model	Name	Reference
INM	Institute for Numerical Mathematics CM3.0	Galin et al. (2003), Diansky et al. (2002)
NCARc	National Center for Atmospheric Research CCSM3	Collins et al. (2004), Smith and Gent (2002)
GFDL0	Geophysical Fluid Dynamics Laboratory CM2.0	GFDLx (2004), Gnanadesikan et al. (2004)
MRI	Meteorological Research Institute CGCM2.3	Shibata et al. (1999) Yukimoto et al. (2001)
CCCma	Canadian Center for Climate Modelling and Analysis CGCM3.1	McFarlane et al. (1992), Flato (2005), Pacanowski et al. (1993)
MIROC-Mid	Model for Interdisciplinary Research on Climate Lower-resolution setup (T42)	developers (2004)
MIROC-Hi	Model for Interdisciplinary Research on Climate Higher-resolution setup (T106)	developers (2004)
HadGem	United Kingdom Meteorological Office HadGem1	Martin et al. (2004), Roberts (2004)

from monthly mean data from year 60 to 80 in the 1%CO_2 perturbed and control simulations. Atmospheric CO_2 concentration reaches double control concentration in 1%CO_2 at year 70. In order to assess the statistical significance of the difference between 2 × CO_2 and 1%CO_2, we calculated the strength of climate feedbacks by taking five different 20-yr segments of the control simulation for 1%CO_2 as a baseline, and calculated the uncertainty range by 90% confidence interval of their mean using the *t*-distribution. We took five 20-yr segments because the shortest control simulation for 1%CO_2 was only 100 yr long. Note that the uncertainty range calculated by this method does not include the effect of uncertainty in the perturbed simulation of 1%CO_2. This is because the number of ensemble members with different initial condition in 1%CO_2 available from PCMDI was small. We confirmed that this effect was small and would not affect our conclusion by using the initial condition ensembles of 1%CO_2 by MIROC-Mid and HadGem (not shown). The uncertainty range was not calculated for MRI because the control simulation data for the analysis was not available from PCMDI. All the results are presented as the time averages for these 20-yr monthly mean data.

In 2 × CO_2, the equilibrium climate sensitivity, $T_{2\times}$, and equilibrium climate feedback parameter, $\lambda_{2\times}$, are defined as

$$T_{2\times} = G_{2\times}/\lambda_{2\times}, \tag{1}$$

where $G_{2\times}$ is the globally averaged adjusted radiative forcing at the tropopause, and $T_{2\times}$ is the globally averaged temperature anomaly in 2 × CO_2. On the other hand, in 1%CO_2, the relationship between the effective climate feedback parameter, $\lambda_{2\times,\mathrm{eff}}$, the globally averaged temperature anomaly, T', and the globally averaged radiative imbalance at TOA, F_{TOA} can be described as

$$F_{\mathrm{TOA}} = G_{1\%} - \lambda_{2\times,\mathrm{eff}} T', \tag{2}$$

where $G_{1\%}$ is the globally averaged adjusted radiative forcing at the tropopause in 1%CO_2 (same as $G_{2\times}$ at year 70 when the atmospheric CO_2 concentration is doubled). By using $\lambda_{2\times,\mathrm{eff}}$ from eq. (2), the effective climate sensitivity, $T_{2\times,\mathrm{eff}}$, can be described as

$$T_{2\times,\mathrm{eff}} = G_{2\times}/\lambda_{2\times,\mathrm{eff}}, \tag{3}$$

which corresponds to the equilibrium climate sensitivity that would be calculated if the climate feedback parameter is fixed to $\lambda_{2\times,\mathrm{eff}}$ (Murphy, 1995).

In this study, we evaluated the ice-albedo feedback, cloud short- (SW) and long-wave (LW) feedback, and ocean heat uptake of 2 × CO_2 and 1%CO_2 of the CMIP3 climate models by using a simple diagnosis of climate feedback analysis. The basic idea of the APRP by Taylor et al. (2007) is similar to that of Yokohata et al. (2005a,b), but the method of Taylor et al. (2007) gives results that are much closer to the PRP calculation than the latter two. As for the cloud LW feedback, the conventional CRF method (Cass et al., 1990) was used for the analysis because it can be calculated easily and the LW APRP method proposed by Yokohata et al. (2005b) does not show a distinct advantage over the LW CRF method (Taylor et al., 2007). Note that the LW CRF is contaminated by non-cloud feedbacks (e.g. Soden et al., 2004). We cannot tell how much of the error should be included in cloud LW feedback by this diagnosis because the accuracy of the LW CRF method has not been examined so far. Ocean heat uptake (OHU) is calculated in the same way as in Yokohata et al. (2005a) as the imbalance of the radiative fluxes of the top of the atmosphere (TOA), since the heat content of atmosphere and land surface is small compared to that of ocean (confirmed by the model output). Since all of these methods of climate feedback processes are based on straightforward calculations using the conventional model output of general circulation models, this scheme is of great help for model intercomparison. The strength of the climate feedback processes is represented in the unit of W m^{-2} K^{-1}, where the anomalies of the radiative fluxes caused by each feedback process are normalized by the globally averaged SAT anomaly.

In this study, we have not considered LW clear-sky feedback, such as the water vapour and lapse-rate feedback, because it is difficult to separate the LW forcing component from the feedback component by the simple scheme of climate feedback diagnosis (Yokohata et al., 2007). Therefore, we leave the difference in the LW clear-sky feedback as a future topic for study and focus instead on the climate feedback processes described above.

3. Climate feedback analysis

3.1. Overview

Figure 1 shows the climate feedback analysis of 2 × CO_2 and 1%CO_2 by the CMIP3 climate models using the method described in Section 2. Each bar represents the SAT anomaly ($T_{2\times}$ in 2 × CO_2 and TCR in 1%CO_2), adjusted radiative forcing at the tropopause, climate feedback parameter ($\lambda_{2\times}$ in 2 × CO_2 and $\lambda_{2\times,\mathrm{eff}}$ in 1%CO_2), ice-albedo feedback (1), cloud SW feedback (2), cloud LW feedback (3) and ocean heat uptake of a particular climate model (4). In addition, cloud SW and LW feedback (2 + 3), ice-albedo plus cloud SW and LW feedback (1 + 2 + 3), and the sum of these feedbacks (1 + 2 + 3 + 4) are also shown. Only the data of adjusted radiative forcing were obtained from the supplementary material of the IPCC AR4 (Randall et al., 2007), and the other data were obtained from the PCMDI data archive. Bars are displayed in the order of the SAT anomaly. Note that the order of the models is slightly different between 2 × CO_2 and 1%CO_2; for example, HadGem is in the eighth position in 2 × CO_2, while it is in the sixth position in 1%CO_2.

It is important to note that the order of radiative forcing is different from that of SAT. This means that the strength of SAT increase is not determined by that of radiative forcing, but by the strength of climate feedback, λ. We found that models with a larger value of SAT anomaly have a smaller value of λ. In

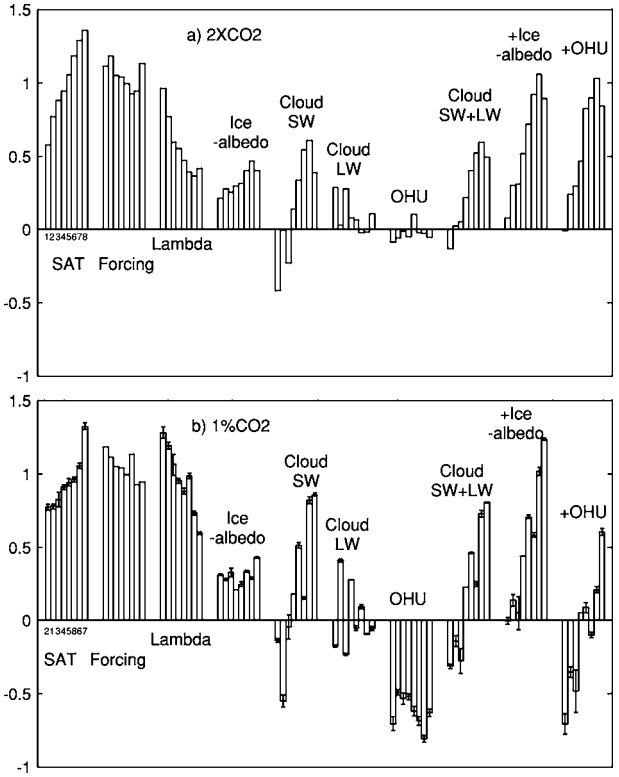

Fig. 1. Climate feedback analysis of (a) the doubled CO_2 experiment ($2 \times CO_2$) and (b) 1% per year CO_2 increase experiment ($1\%CO_2$) by the method described in the text. Variables shown are the surface air temperature anomaly (SAT, unit is K, a factor of 0.3 is applied in $2 \times CO_2$, and a factor of 0.5 is applied in $1\%CO_2$), the adjusted radiative forcing at the tropopause (unit is W m^{-2}), the climate feedback parameter (λ, a factor of 0.5 is applied in $2 \times CO_2$ and $1\%CO_2$) defined in eqs (1) and (3), ice-albedo feedback, cloud SW feedback, cloud LW feedback, and ocean heat uptake (OHU). The term 'Cloud SW+LW' represents the sum of the cloud SW and LW feedback, '+ice-albedo' represents the sum of the cloud SW and LW feedback and ice-albedo feedback, and '+OHU' represents the sum of the cloud SW and LW feedback, ice-albedo feedback, and OHU. All variables except the SAT anomaly and the adjusted radiative forcing have the unit of W m^{-2} K^{-1}. Each bar represents a climate model from CMIP3, and the bars are displayed in the same order for all the variables in $2 \times CO_2$ and $1\%CO_2$. Error bar in $1\%CO_2$ is the uncertainty range calculated by using the different segments of control simulations as a baseline. The models are (1) INM, (2) NCARc, (3) GFDL0, (4) MRI, (5) CCCma, (6) MIROC-Mid, (7) MIROC-Hi and (8) HadGem, as described in Table 1. Note that the order of the models in $2 \times CO_2$ is different from that in $1\%CO_2$.

addition, the order of the sum of the feedbacks ($1 + 2 + 3 + 4$) is almost the same as the opposite order of λ (and the order of the SAT anomaly) in $2 \times CO_2$ and $1\%CO_2$. This means that the sum of the ice-albedo, cloud SW and LW feedback, and OHU determines the difference in the SAT anomaly among climate models. One of the exceptions is that in $2 \times CO_2$, the sum of feedback and λ of HadGem is smaller than that of MIROC-Mid and MIROC-Hi while the SAT anomaly of HadGem is the largest. This is possibly because the radiative forcing of HadGem is larger than that of MIROC-Mid or MIROC-Hi. In $1\%CO_2$, the sum of feedback and λ of HadGem is smaller compared to those of MRI and CCCma, possibly because of the larger radiative forcing, and those of GFDL0 is smaller than those of INM, which has relatively large uncertainty ranges.

As shown in Figure 1, the largest difference among climate models is cloud SW feedback, and the next largest difference among models is cloud LW feedback. This result is consistent with Soden and Held (2006), where major climate feedback processes were diagnosed by a scheme of the radiative kernel method. In both $2 \times CO_2$ and $1\%CO_2$, all models have positive ice-albedo feedback.

In $1\%CO_2$, OHU is generally large and negative, which suppresses the increase in SAT owing to heat absorption by the ocean, while OHU is negligible in $2 \times CO_2$ because equilibrated states have been achieved. Whereas studies so far (Raper et al., 2002) have suggested that the AOGCMs with larger $T_{2\times}$ tend to have larger ocean heat uptake efficiency by using the climate models from the second phase of the Coupled Model Intercomparison Project, this relation cannot be seen in Fig. 1. In addition, Yokohata et al. (2007) showed that there is a good correlation between OHU and globally averaged mixed layer depth (MLD) using two versions of an AOGCM with different model resolutions, MIROC-Hi and MIROC-Mid, but the correlation between OHU and MLD is not good in the CMIP3 climate models used here (not shown). This is possibly because the processes which determine OHU are different among the CMIP3 climate models (such as the southern hemisphere westerlies, e.g. Russel et al., 2006).

3.2. *Comparison of equilibrium and transient responses*

Here, we compared the equilibrium responses in $2 \times CO_2$ and transient responses in $1\%CO_2$. In Table 2, the values of climate

Table 2. Equilibrium climate sensitivity ($T_{2\times}$), adjusted radiative forcing at the tropopause (G), climate feedback parameter of $2 \times CO_2$ ($\lambda_{2\times}$) and $1\%CO_2$ ($\lambda_{2\times,\mathrm{eff}}$), and effective climate sensitivity ($T_{2\times,\mathrm{eff}}$)

Model	$T_{2\times}$	G	$\lambda_{2\times}$	$\lambda_{2\times,\mathrm{eff}}$	$T_{2\times,\mathrm{eff}}$
INM	1.92	3.71	1.93	1.90	1.96
NCARc	2.57	3.95	1.54	1.85	2.13
GFDL0	2.93	3.50	1.19	1.59	2.20
MRI	3.15	3.47	1.10	1.38	2.51
CCCma	3.52	3.32	0.94	1.14	2.90
MIROC-Mid	3.95	3.09	0.78	0.66	4.70
MIROC-Hi	4.29	3.14	0.73	0.56	5.63
HadGem	4.53	3.78	0.85	1.28	2.95

Note: The definitions of the variables are given in the text.

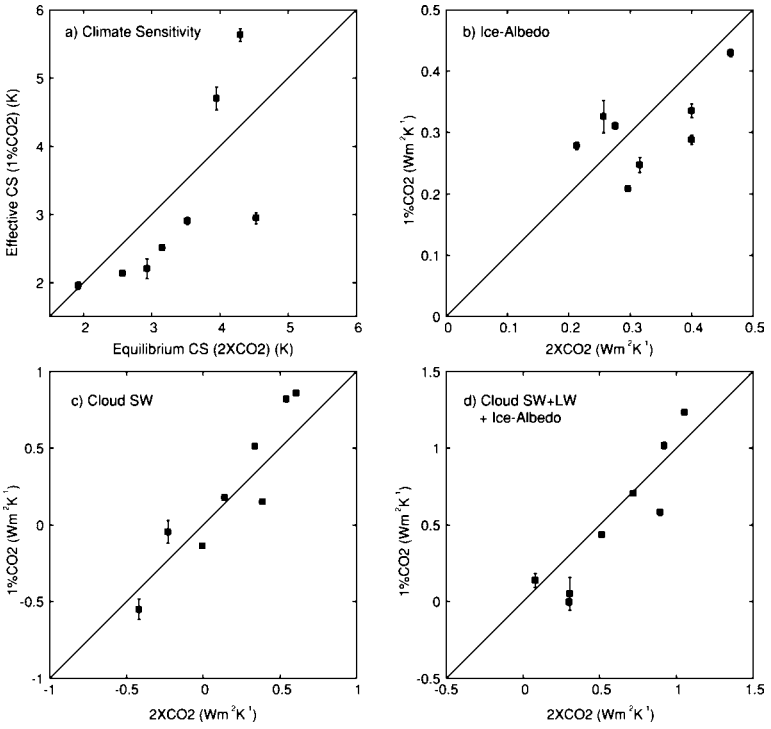

Fig. 2. Scatter plot of (a) equilibrium and effective climate sensitivity ($T_{2\times}$ and $T_{2\times,\mathrm{eff}}$), (b) ice-albedo feedback, (c) cloud SW feedback and (d) sum of ice-albedo and cloud SW and LW feedback in $2 \times CO_2$ and $1\%CO_2$ of the CMIP3 climate models. Each point shows the result of one climate model, the horizontal axis represents the results from $2 \times CO_2$, and the vertical axis represents those from $1\%CO_2$. Error bar for vertical axis is the uncertainty range calculated by using the different segments of control simulations as a baseline.

sensitivities, adjusted radiative forcings, and climate feedback parameters defined in eqs (1) and (3) are summarized. In general, equilibrium and effective climate sensitivities ($T_{2\times}$ and $T_{2\times,\mathrm{eff}}$) are different. The former is lager than the latter in some models (NCARc, GFDL0, MRI, CCCma and HadGem), and vice versa in other models (INM, MIROC-Mid and MIROC-Hi). As a result, the spread of $T_{2\times}$ among climate models (1.92–4.52 K) expanded in $T_{2\times,\mathrm{eff}}$ (1.82–5.12 K). We can see this feature more clearly from the scatter plot of $T_{2\times}$ and $T_{2\times,\mathrm{eff}}$) shown in Fig. 2a.

Next, we investigated the factors which cause the difference between $T_{2\times}$ and $T_{2\times,\mathrm{eff}}$. In order to investigate this factor, we calculated the climate sensitivity that would occur if the particular climate feedback of $2 \times CO_2$ was replaced by that of $1\%CO_2$ as follows. For example, we consider a case when the ice-albedo feedback (unit is W m^{-2} K^{-1}) in $2 \times CO_2$ is replaced to that in $1\%CO_2$. The climate feedback parameters, $\lambda_{2\times}$ and $\lambda_{1\%}$, can be described as

$$\lambda_{2\times} = -\gamma_{\mathrm{res,2x}} - \gamma^{\mathrm{sw}}_{\mathrm{sfc,2x}}$$
$$\lambda_{1\%} = -\gamma_{\mathrm{res},1\%} - \gamma^{\mathrm{sw}}_{\mathrm{sfc},1\%},$$

where γ_{res} is the climate feedback processes except $\gamma^{\mathrm{sw}}_{\mathrm{sfc}}$. If $\gamma^{\mathrm{sw}}_{\mathrm{sfc,2x}}$ is replaced by $\gamma^{\mathrm{sw}}_{\mathrm{sfc},1\%}$ in $2 \times CO_2$, the climate feedback parameter becomes

$$\lambda'_{2\times} = -\gamma_{\mathrm{res,2x}} - \gamma^{\mathrm{sw}}_{\mathrm{sfc},1\%}$$
$$= \lambda_{2\times} - \Delta\gamma^{\mathrm{sw}}_{\mathrm{sfc}},$$

where $\Delta\gamma^{\mathrm{sw}}_{\mathrm{sfc}}$ is the difference in the $\gamma^{\mathrm{sw}}_{\mathrm{sfc}}$ between $1\%CO_2$ and $2 \times CO_2$. Therefore, the difference between $T_{2\times}$ and the climate sensitivity that would occur if the ice-albedo feedback of $2 \times CO_2$ is replaced by that of $1\%CO_2$ is calculated as

$$\Delta T_{2\times} \text{ by ice albedo feedback} = \frac{G_{2\times}}{\lambda_{2\times}} - \frac{G_{2\times}}{\lambda_{2\times} - \Delta\gamma^{\mathrm{sw}}_{\mathrm{sfc}}}. \quad (4)$$

If the ice-albedo feedback of $2 \times CO_2$ is larger than that of $1\%CO_2$ ($\Delta\gamma^{\mathrm{sw}}_{\mathrm{sfc}} < 0$), $\Delta T_{2\times}$ by the ice-albedo feedback followed by eq. (4) becomes positive. $\Delta T_{2\times}$ by the particular feedback was estimated in the same way as Williams and Tselioudis (2007), where the observationally constrained $T_{2\times}$ was calculated from the difference in the net CRF between the model result and the data constrained by observation.

In Table 3, the difference between $T_{2\times}$ and $T_{2\times,\mathrm{eff}}$($\Delta T_{2\times}$), $\Delta T_{2\times}$ by the ice-albedo feedback, cloud SW and LW feedback, and by the sum of the three feedbacks. As shown in Table 3, $\Delta T_{2\times}$ becomes more than 1 K in some models. In general, the value of $\Delta T_{2\times}$ is close to $\Delta T_{2\times}$ by the sum of ice-albedo and cloud feedback. Therefore, a large part of $\Delta T_{2\times}$ can be explained by the difference in the ice-albedo and cloud feedback between $2 \times CO_2$ and $1\%CO_2$. In Table 3, the values of $\Delta T_{2\times}$ by the cloud SW feedback are larger than those of $\Delta T_{2\times}$ by the ice-albedo or cloud LW feedback in many models, and thus the largest contribution to $\Delta T_{2\times}$ is $\Delta T_{2\times}$ by the cloud SW feedback. In MIROC-Mid and MIROC-Hi, these values become more than 2 K. $\Delta T_{2\times}$ by ice-albedo feedback is also large, and this value becomes about 0.4 K, which corresponds to ~10% of $T_{2\times}$. Note

Table 3. Difference in the equilibrium and effective climate sensitivity ($\Delta T_{2\times} = T_{2\times} - T_{2\times,\mathrm{eff}}$), contribution to $\Delta T_{2\times}$ by ice-albedo feedback, cloud SW feedback, cloud LW feedback and the sum of ice-albedo and cloud SW and LW feedback (unit is K)

Model	$\Delta T_{2\times}$ $(T_{2\times} - T_{2\times,\mathrm{eff}})$	$\Delta T_{2\times}$ by Ice-albedo	$\Delta T_{2\times}$ by Cloud SW	$\Delta T_{2\times}$ by Cloud LW	$\Delta T_{2\times}$ by Ice+Cloud
INM	−0.03	−0.07	0.12	−0.13	−0.05
NCARc	0.44	−0.06	0.20	0.30	0.42
GFDL0	0.73	−0.18	−0.53	0.88	0.52
MRI	0.64	0.23	−0.12	−0.68	0.21
CCCma	0.62	0.24	−0.80	0.39	0.04
MIROC-Mid	−0.74	0.50	−2.18	0.32	−0.56
MIROC-Hi	−1.34	0.19	−2.24	0.22	−1.37
HadGem	1.58	0.33	0.99	0.06	1.23

Note: The definition of $\Delta T_{2\times}$ by the particular feedback is given in the text.

that $\Delta T_{2\times}$ by cloud LW feedback should include an error to some extent owing to the problem in the CRF method.

Figure 2 shows a comparison of climate feedback processes for $2 \times CO_2$ and $1\%CO_2$ by the same climate models. Error bars represent the uncertainty ranges of $1\%CO_2$ calculated by the 90% confidence interval using the different segment of control simulations as a baseline. In almost all the cases, the differences between $2 \times CO_2$ and $1\%CO_2$ are larger than the uncertainty ranges of $1\%CO_2$, which suggests that the differences in the effective climate sensitivity and climate feedback processes between $2 \times CO_2$ and $1\%CO_2$ are statistically significant. The ice-albedo feedback of $2 \times CO_2$ tends to be larger than that of $1\%CO_2$. The possible mechanisms for this difference are investigated in Section 3.3. Cloud SW feedback of $2 \times CO_2$ are also different from those of $1\%CO_2$ (Fig. 2c, note that the range of the figures is larger than in Figure 2a because the spread of cloud feedback between climate models is larger than that of ice-albedo feedback). The details of the difference in cloud SW feedback are discussed in Section 3.4.

3.3. *Ice-albedo feedback*

Globally averaged values of ice-albedo feedback in the two experiments are shown in Table 4. The ice-albedo feedback diagnosed by the APRP method includes the effects of changes in snow cover over land and sea-ice. According to Taylor et al. (2007), the error of the globally averaged value of ice-albedo feedback calculated by the APRP from the PRP method is about 10%. Table 4 shows that the differences in the ice-albedo feedback between $2 \times CO_2$ and $1\%CO_2$ are larger than 10% for both experiments in most of the models (except NCARc and MIROC-Hi). In addition, the difference between $2 \times CO_2$ and $1\%CO_2$ is larger than the uncertainty range of $1\%CO_2$ in all the models.

Latitudinal distributions of the ice-albedo feedback in $2 \times CO_2$ and $1\%CO_2$ are shown in Fig. 3. The differences in ice-albedo feedback between two experiments are caused mainly at the southern high latitudes from about 50°S to 80°S. Ice-albedo feedback in the southern high latitudes is determined by the

Table 4. Globally averaged value of the ice-albedo and cloud SW feedback (unit: W m^{-2} K^{-1}). The results of $2 \times CO_2$, $1\%CO_2$, their difference ($\Delta = 2 \times CO_2$ - $1\%CO_2$), and the uncertainty range of $1\%CO_2$ (in the parenthesis) are shown

Model	Ice-albedo feedback			Cloud SW feedback		
	$2 \times CO_2$	$1\%CO_2$	Δ	$2 \times CO_2$	$1\%CO_2$	Δ
INM	0.21	0.28	−0.06 (0.01)	−0.42	−0.55	0.13 (0.07)
NCARc	0.28	0.31	−0.03 (0.01)	−2E-3	−0.14	0.13 (0.01)
GFDL0	0.26	0.33	−0.06 (0.03)	−0.23	−0.04	−0.18 (0.08)
MRI	0.30	0.21	0.08 (—)	0.14	0.18	−0.03 (—)
CCCma	0.32	0.25	0.06 (0.01)	0.34	0.51	−0.17 (0.02)
MIROC-Mid	0.40	0.29	0.11 (0.01)	0.54	0.82	−0.28 (0.02)
MIROC-Hi	0.46	0.43	0.03 (0.01)	0.61	0.86	−0.25 (0.01)
HadGem	0.40	0.34	0.06 (0.01)	0.39	0.15	0.24 (0.01)

Note: The values with $|\Delta| > 0.10$ are underlined.

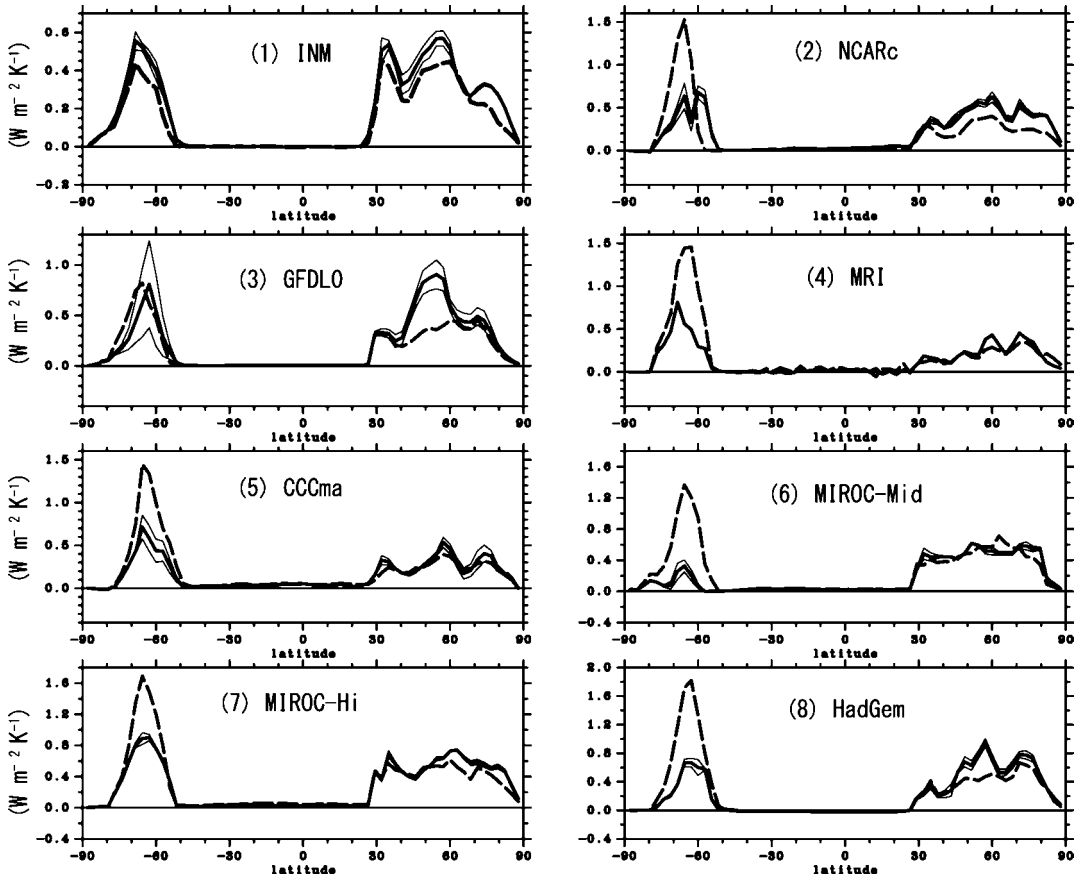

Fig. 3. Latitudinal distribution of ice-albedo feedback (unit: W m^{-2} K^{-1}). Thick dashed curve represents the result of 2 × CO_2, thick solid curve represents 1%CO_2, and thin curves represent the uncertainty range of 1%CO_2. Models with numbers from (1) to (8) correspond to the CMIP3 climate models described in Table 1. The factor of the cosine of the latitudes is multiplied in order to consider the areal weight.

response of sea ice in the Southern Ocean. Note that in some models (INM and GFDL0), the uncertainty range of ice-albedo feedback in 1%CO_2 becomes large especially at the Southern Ocean. This is because the variability of sea ice in the control simulation is large in these models. In other models, however, the uncertainty range is smaller than the difference between 1%CO_2 and 2 × CO_2.

Spelman and Manabe (1984) and Rind et al. (1995) have shown that initial distributions (i.e. distributions in the control experiments) of sea ice is an important factor that controls the sea ice responses to CO_2 increase in the Southern Ocean. Yokohata et al. (2007) have investigated the differences in ice-albedo feedback between MIROC-Hi and MIROC-Mid and found that the initial distribution of sea ice at the Southern Ocean of the former is larger than that of the latter, and thus the ice-albedo feedback of the former becomes larger than that of the latter.

Figure 4 shows the differences in the sea ice anomalies and the initial distributions of sea ice between 2 × CO_2 and 1%CO_2. Here, the sea ice distribution is shown as surface albedo calculated as the ratio of the upward to downward SW radiation at the surface, since the areas with sea ice have very high albedo compared to the areas without them. In many models (GFDL, MRI, CCCma, MIROC-Mid, MIROC-Hi and HadGem), the sea ice anomaly in 2 × CO_2 is larger (i.e. the ice-albedo feedback is larger) than that in 1%CO_2, and this is also true for the initial sea ice distributions. As shown in Fig. 4, the difference in the sea ice anomaly between 2 × CO_2 and 1%CO_2 is larger over the area where the difference in initial sea ice distribution is larger in these models. These results indicate that the ice-albedo feedback of 2 × CO_2 has become larger than that of 1%CO_2 in these models because of the larger initial sea ice distributions in the former.

In 2 × CO_2, an artificial heat flux is applied in order to consider the effects of ocean heat transport in ASGCMs. On the other hand, in 1%CO_2, physical processes in the ocean-sea ice system are explicitly considered in AOGCMs. In general, the sea ice scheme in AOGCMs is more realistic than that in ASGCMs because the dynamical interaction between the sea ice and ocean is considered adequately in AOGCMs (e.g. Johns et al., 2006). It is, therefore, reasonable to assume that the behaviour of the ocean-sea ice system in 1%CO_2 is more reliable than that in 2 × CO_2. Figure 5 shows the initial distribution of sea ice in

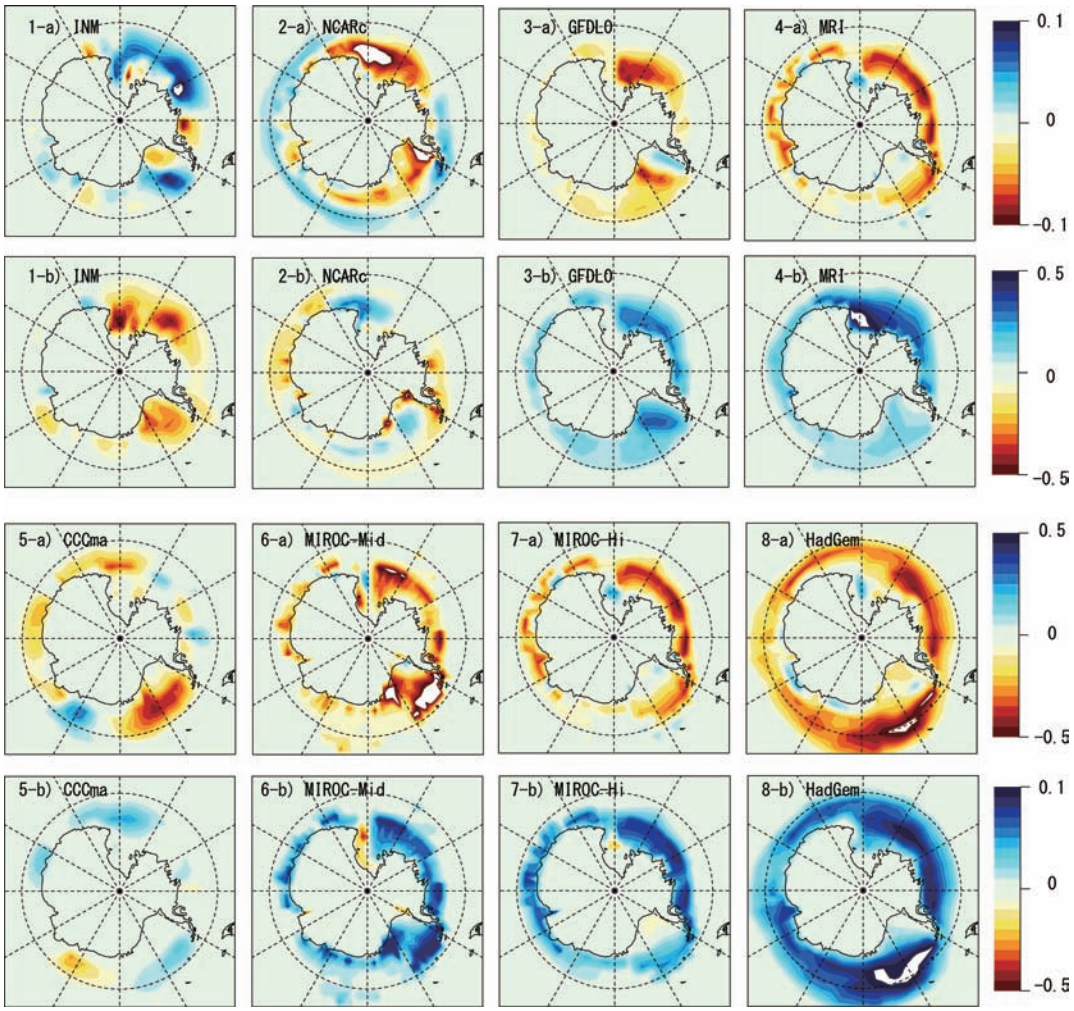

Fig. 4. From (a-1) to (a-8): Differences in sea ice anomaly between $2 \times CO_2$ and $1\%CO_2$. The anomalies are normalized by the globally averaged SAT anomaly. From (b-1) to (b-8): difference in the initial sea ice distribution between $2 \times CO_2$ and $1\%CO_2$. Numbers from (1) to (8) correspond to the CMIP3 climate models described in Table 1. Red in (a) figures indicates that the sea ice anomaly of $2 \times CO_2$ is larger than that of $1\%CO_2$, and blue in (b) figures indicates that the initial sea ice distribution of $2 \times CO_2$ is larger than that of $1\%CO_2$. Values represented here are the surface albedo (ratio of upward SW radiation to the downward SW radiation), which represents the distribution of sea ices because the regions with sea ices have high surface albedo. Averages of the summer season (December, January, and February) are shown because the ice-albedo feedback is determined during the summer season when there is enough solar radiation.

$2 \times CO_2$ and $1\%CO_2$. From a practical perspective, the initial distributions of sea ice in $1\%CO_2$ generally show better agreement with observations than those in $2 \times CO_2$.

It is interesting to note that in $2 \times CO_2$, the initial extent of sea ice over the Southern Ocean is overestimated in many models compared to observations and $1\%CO_2$ (Fig. 5). One of the factors which suppresses sea-ice formation at the Southern Ocean in AOGCMs is deep convection (e.g. Yokohata et al., 2007). One possible reason why the sea ice distributions in ASGCMs cannot be represented properly is that dynamical interactions between the sea ice and ocean cannot be described properly by the procedure of giving artificial heat flux.

Another possible factor that could cause the difference in the ice-albedo feedback between $2 \times CO_2$ and $1\%CO_2$ is the difference in the SAT response between the two experiments. Figure 6 shows the latitudinal distribution of SAT anomalies normalized by the globally averaged SAT anomalies, which represent the latitudinal distribution of the relative strength of the SAT increase. Temperature increase at the Southern Ocean in $2 \times CO_2$ is larger than that in $1\%CO_2$, since the OHU of $2 \times CO_2$ is almost negligible while that of $1\%CO_2$ is large at the Southern Ocean, over the region where the mixed layer depth of the ocean is large (Yokohata et al., 2007). The relative strength of the temperature increase at the Southern Ocean is larger in $2 \times CO_2$

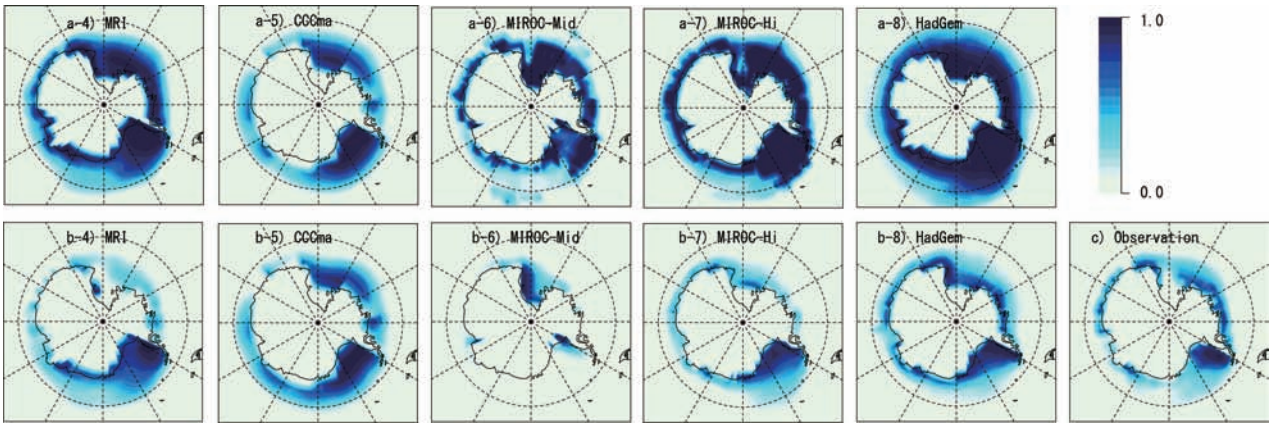

Fig. 5. From (a-4) to (a-8): Initial sea ice distribution of $2 \times CO_2$ (20-year averages of the control experiments when equilibrated state is achieved). From (b-4) to (b-8): that of $1\%CO_2$ (averages over the 20 yr of the control simulation). (c) Observation of sea ice distribution from 1981 to 2000 by Rayner et al. (2003). Numbers (4) to (8) correspond to the CMIP3 climate models described in Table 1. Here the sea ice distribution is presented as sea ice concentration, the fraction of the area where the sea ice exists. Only the results of the models which have both $2 \times CO_2$ and $1\%CO_2$ data in the PCMDI data archive are shown.

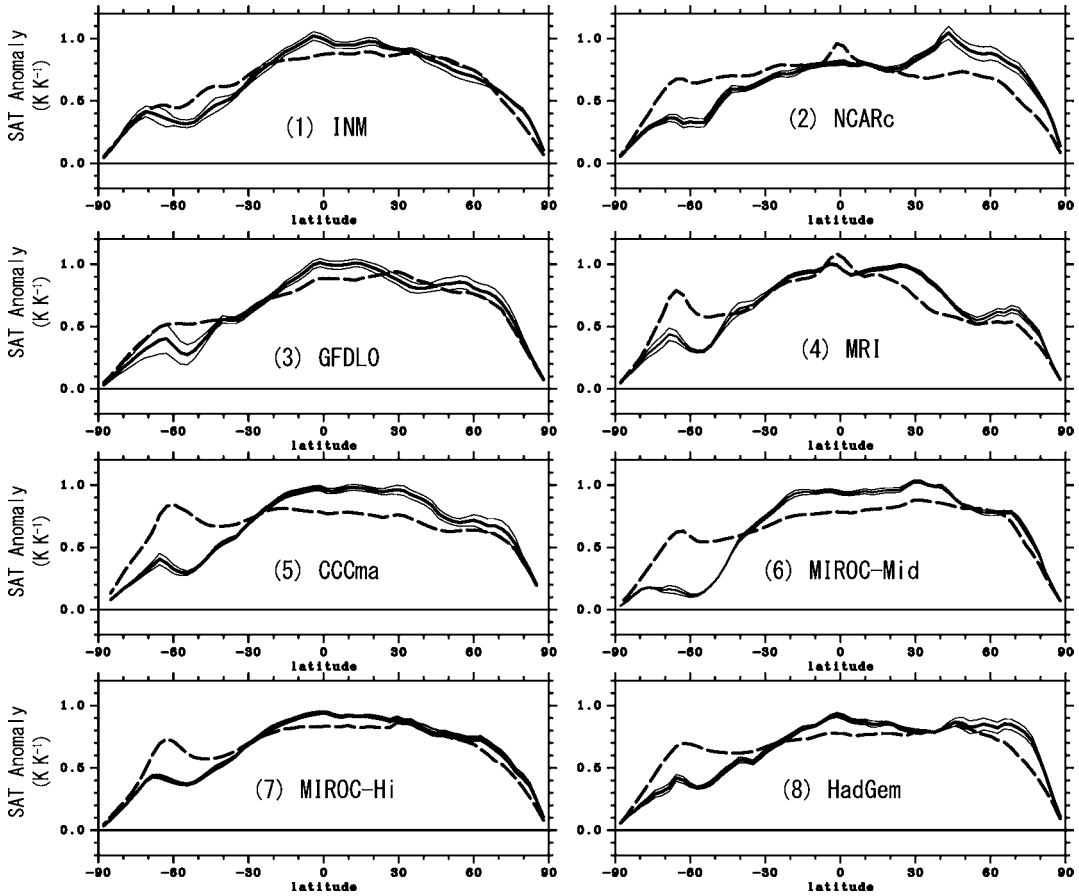

Fig. 6. Same as Fig. 3 but for the SAT anomaly normalized by the globally averaged SAT anomalies (unit is K K^{-1}).

than in 1%CO_2, which may enhance the ice-albedo feedback of 2 × CO_2 more than that of 1%CO_2.

3.4. Cloud SW feedback

Table 4 shows the globally averaged value of cloud SW feedback in 2 × CO_2 and 1%CO_2. Taylor et al. (2007) have demonstrated that the error of the cloud SW feedback diagnosed by the APRP method from the PRP method is about 7%. As shown in Table 4, the difference in the cloud SW feedback between 2 × CO_2 and 1%CO_2 is more than 7% for both of the experiments in all models. In addition, the difference between 2 × CO_2 and 1%CO_2 is larger than the uncertainty range of 1%CO_2 in all the models.

In general, the cloud SW feedback of the models with relatively small $T_{2\times}$ (INM, NCARc and GFDL0) are negative, and those of the models with relatively large $T_{2\times}$ (MRI, CCCma, MIROC-Mid, MIROC-Hi and HadGem) are positive, which is consistent with the results of previous works (e.g. Bony and Dufresne, 2005; Webb et al., 2006; Williams and Tselioudis, 2007).

Latitudinal distributions of cloud SW feedback in 2 × CO_2 and 1%CO_2 are shown in Fig. 7. The strength and latitudinal distribution is significantly different among climate models. Models with very small SAT anomaly, that is, INM and NCARc, have negative cloud SW feedback at almost all the latitudes. In other models with a relatively large SAT anomaly (i.e. MRI, CCCma, MIROC-Mid, MIROC-Hi and HadGem), the cloud SW feedback at low-to-middle latitudes (<40–50°) is positive and those at middle-to-high latitudes (>40–50°) negative or small positive.

In Table 5, we investigated the regional contribution to the differences in cloud SW feedback between 2 × CO_2 and 1%CO_2. In many models (INM, NCARc, GFDL0, MIROC-Mid, MIROC-Hi and HadGem), the difference appeared at the mid-to-high latitudes (>30°). On the other hand, in some models (NCARc, GFDL0, CCCma and MIROC-Hi), the differences are appeared at the low latitudes (<30°). The difference between 2 × CO_2 and 1%CO_2 is larger than the uncertainty range of 1%CO_2 in all the models.

In the models with the difference at mid-to-high latitudes (INM, GFDL0 and HadGem), the cloud SW feedback of

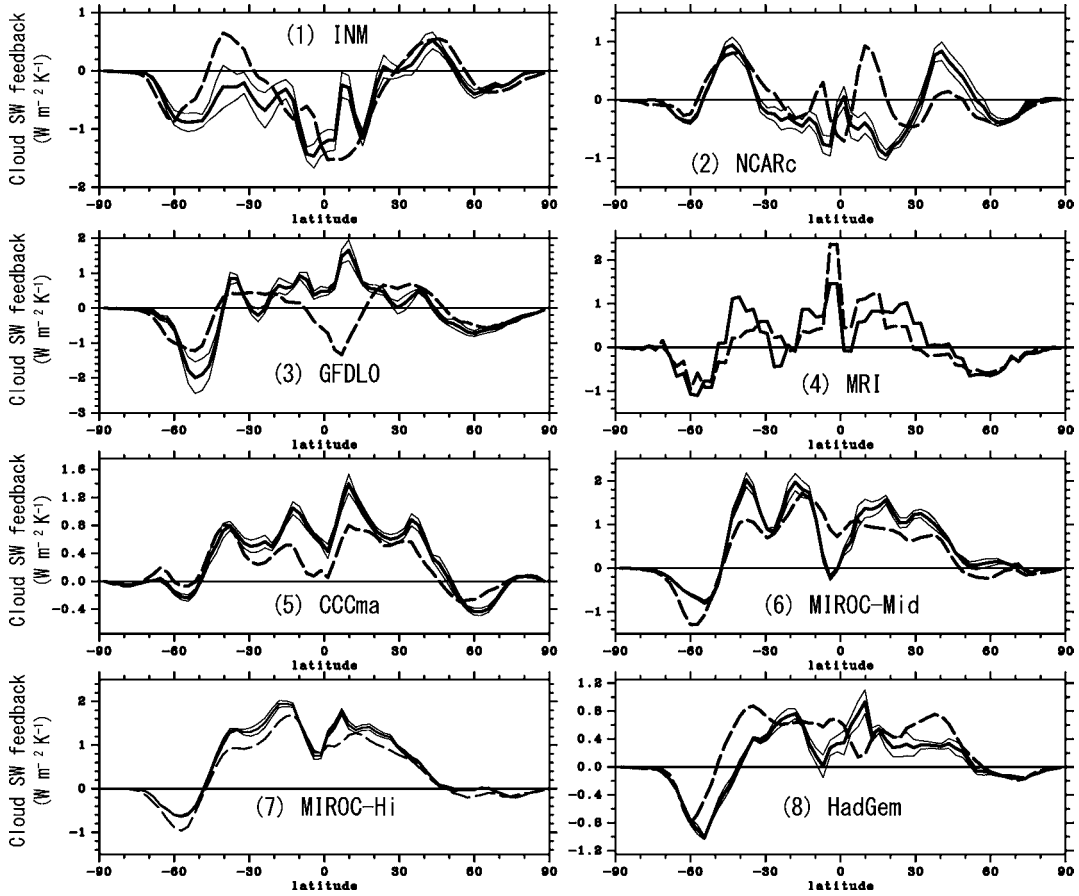

Fig. 7. Same as Fig. 3 but for the cloud SW feedback (unit is W m^{-2} K^{-1}).

Table 5. The cloud SW feedback of $2 \times CO_2$, $1\%CO_2$, their difference (Δ), and the uncertainty range of $1\%CO_2$ in the parenthesis, averaged over the low ($< 30^\circ$) and mid-to-high ($< 30^\circ$) latitudes

Model	Latitude $<30^\circ$			Latitude $>30^\circ$		
	$2 \times CO_2$	$1\%CO_2$	Δ	$2 \times CO_2$	$1\%CO_2$	Δ
INM	−0.38	−0.35	−0.03 (0.02)	−0.03	−0.20	0.17 (0.04)
NCARc	−0.03	−0.25	0.22 (0.02)	0.03	0.12	−0.09 (0.03)
GFDL0	−0.01	0.30	−0.31 (0.03)	−0.22	−0.36	0.14 (0.06)
MRI	0.35	0.29	0.05 (—)	−0.22	−0.12	−0.10 (—)
CCCma	0.23	0.40	−0.18 (0.02)	0.11	0.10	0.01 (0.01)
MIROC-Mid	0.54	0.57	−0.03 (0.04)	−0.01	0.25	−0.25 (0.02)
MIROC-Hi	0.60	0.73	−0.13 (0.01)	−0.01	0.12	−0.12 (0.01)
HadGem	0.28	0.24	0.04 (0.01)	0.10	−0.09	0.20 (0.01)

Note: The values with $|\Delta| > 0.10$ are underlined.

$2 \times CO_2$ was generally larger than that of $1\%CO_2$ (Table 5), especially at the southern hemisphere (Fig. 7). These differences at the mid-to-high latitudes may have been caused by the shift in storm track (e.g. Tsushima et al., 2006). The shift in storm track is related to the change in baroclinicity (Yin, 2005) represented by the maximum growth rate of baroclinic instabilities (Lindzen and Farrell, 1980) as $0.31gN^{-1}T^{-1}|\partial T/\partial y|$, where T is the zonal mean temperature and N is the Brunt–Vaisara frequency calculated using T. The temperature increase in $1\%CO_2$ is generally smaller than $2 \times CO_2$ at the high latitudes and vice versa at the middle latitudes owing to the ocean heat uptake especially in the southern hemisphere (Fig. 6). Because of this, the anomaly in the temperature gradient of $1\%CO_2$ is larger and thus the increase in the baroclinicity is larger than in $2 \times CO_2$. As shown in Fig. 8, the increase in the baroclinicity in $1\%CO_2$ is larger than in $2 \times CO_2$, which correspond to the more negative cloud SW feedback in these models. These results are consistent with that of Senior and Mitchell (2000).

On the other hand, MIROC-Mid and MIROC-Hi showed the difference at the mid-to-high latitudes but the cloud SW feedback of $1\%CO_2$ was larger (smaller negative) than that of $2 \times CO_2$. In this latitudinal region, cloud water increases due to the melting of cloud ices (Senior and Mitchell, 1993; Tsushima et al., 2006). The ratio of cloud water and ice in the MIROC model is diagnosed from the atmospheric temperature (Ogura et al., 2008). As shown in Fig. 9, the cloud water increase at the high latitudes (especially at the southern hemisphere) in $2 \times CO_2$ is larger than that in $1\%CO_2$. The atmospheric temperature response of $2 \times CO_2$ is also larger than that of $1\%CO_2$ (Fig. 9). This feature of cloud water increase at high latitudes can be seen in other models (Fig. 7 in Tsushima et al., 2006). The fact that the amount of cloud water increase in MIROC is relatively large compared to other models may cause the cloud SW feedback to be negative (and cause the difference between $2 \times CO_2$ and $1\%CO_2$) only in the MIROC models.

As for the difference in cloud SW feedback at the low latitudes, Boer and Yu (2003) demonstrated that the difference in SST response between the ASGCMs and AOGCMs due to the ocean heat transport possibly causes the difference in tropical feedback related to moisture and cloud: the larger SST anomaly (El-Nino like response) in AOGCMs possibly causes more positive feedback. In addition, Williams et al. (2006) demonstrated that the change in saturated stability (the difference in saturated equivalent potential temperature at 700 hPa and at the surface) is closely correlated to the change in low cloud because unstable conditions are likely to generate less cloud (shallow convection is not capped so strongly). Table 6 shows the differences in cloud SW feedback ($\Delta\gamma^{sw}_{cld}$), SAT anomaly, and saturated stability anomaly ($\Delta\theta_{es}$) between $2 \times CO_2$ and $1\%CO_2$ at low latitudes($<30^\circ$). In addition, in order to isolate the effect of the difference in SAT anomaly on the cloud SW feedback, we calculate the cloud SW feedback normalized by the local ($<30^\circ$ latitude) SAT anomaly as

$$\gamma^{sw}_{cld,local} = F^{sw}_{cld,low}/T'_{low}, \tag{5}$$

where $T_{low}{}'$ and $F^{sw}_{cld,low}$ are the low-latitude average of the SAT anomaly and cloud contribution to the TOA SW anomaly. Note that the cloud SW feedback, γ^{sw}_{cld}, is normalized by the globally averaged SAT anomaly.

As shown in Table 6, $\Delta\gamma^{sw}_{cld,local}$ is not negligible compared to the value of $\Delta\gamma^{sw}_{cld}$. This means that the difference in the SAT anomaly cannot explain the difference in cloud SW feedback between $2 \times CO_2$ and $1\%CO_2$. As for NCARc and MIROC, the sign of $\Delta\gamma^{sw}_{cld}$ is consistent with that of $\Delta\theta_{es}$: the anomaly in saturated stability of $2 \times CO_2$ is smaller (less stable) and the cloud SW feedback is larger (less cloud) than that of $1\%CO_2$, and vice versa. In addition, $\Delta\theta_{es}$ is larger than the uncertainty range of $1\%CO_2$. On the other hand, $\Delta\gamma^{sw}_{cld}$ cannot be explained by $\Delta\theta_{es}$ in GFDL0 and CCCma. In these models, different factors other than the saturated stability cause the difference in cloud SW feedback between $2 \times CO_2$ and $1\%CO_2$. We also performed the

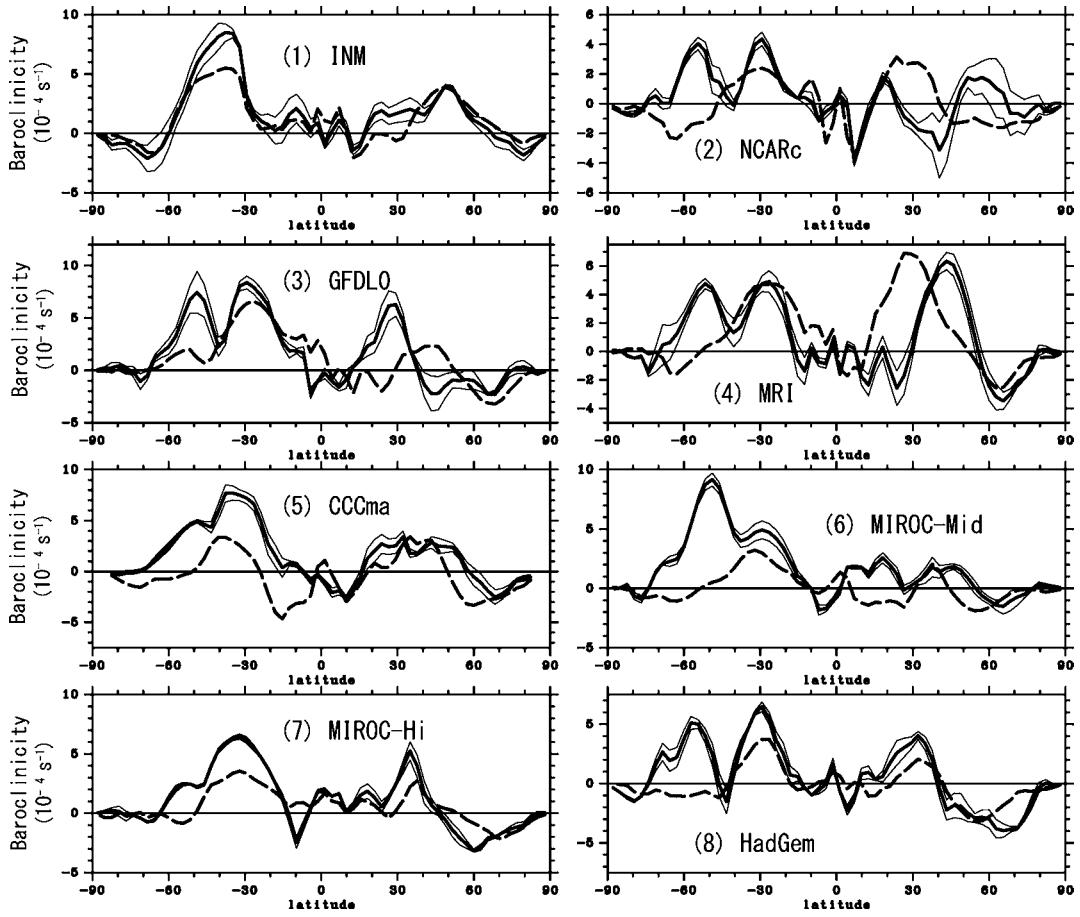

Fig. 8. Same as Fig. 3 but for the anomaly in baroclinicity (unit is s^{-1}). Values of the maximum growth rate of baroclinic instabilities averaged over the troposphere (from the surface to 200 hPa) are shown.

same analysis as that in Bony et al. (2004), and found that the difference in the thermodynamic component of cloud changes between $2 \times CO_2$ and $1\%CO_2$ is an important factor for the difference in cloud SW feedback at low latitudes (not shown). This result that the thermodynamic component plays an important roll is consistent with that of Bony et al. (2004). The mechanisms which cause the difference in the thermodynamic component between $2 \times CO_2$ and $1\%CO_2$ should be investigated in a future study.

4. Summary and discussions

Climate feedback processes were diagnosed by using the results of equilibrium ($2 \times CO_2$) experiments by ASGCMs and transient ($1\%CO_2$) experiments by AOGCMs in the CMIP3 climate models. In general, the total climate feedback parameters of $2 \times CO_2$ and $1\%CO_2$, $\lambda_{2\times}$ and $\lambda_{2\times,\mathrm{eff}}$, are different. Namely, the equilibrium climate sensitivity, $T_{2\times}$, is different from the effective climate sensitivity, $T_{2\times,\mathrm{eff}}$, diagnosed from $1\%CO_2$ at the time of the atmospheric doubled CO_2 condition (Table 2 and Fig. 2a). In some models (NCARc, GFDL0, MRI, CCCma and HadGem), $T_{2\times}$ is larger than $T_{2\times,\mathrm{eff}}$, and vice versa in the other models (INM, MIROC-Mid and MIROC-Hi). The difference between $T_{2\times}$ and $T_{2\times,\mathrm{eff}}(\Delta T_{2\times})$ is up to 1.7 K in these models. While the range of $T_{2\times}$ is from 1.92 to 4.52 K, the range of $T_{2\times,\mathrm{eff}}$ becomes larger, from 1.96 to 5.63 K.

According to our climate feedback analysis by the APRP method, a large part of the $\Delta T_{2\times}$ can be explained by ice-albedo feedback and cloud feedback. The largest contribution to $\Delta T_{2\times}$ is that by the cloud SW feedback, which is up to about 2 K in some models (Table 3). The contribution to $\Delta T_{2\times}$ by ice-albedo feedback is about 0.4 K.

The difference in ice-albedo feedback between $2 \times CO_2$ and $1\%CO_2$ mainly comes from the Southern Ocean. This is possibly because the initial sea ice distribution is different between $2 \times CO_2$ and $1\%CO_2$. The initial sea ice distribution of $2 \times CO_2$ tends to be larger than that of $1\%CO_2$, which causes the overestimation of ice-albedo feedback in $2 \times CO_2$ compared to $1\%CO_2$. In practical perspective, the initial sea ice distribution of $1\%CO_2$ shows better agreement with observation than $2 \times CO_2$, possibly

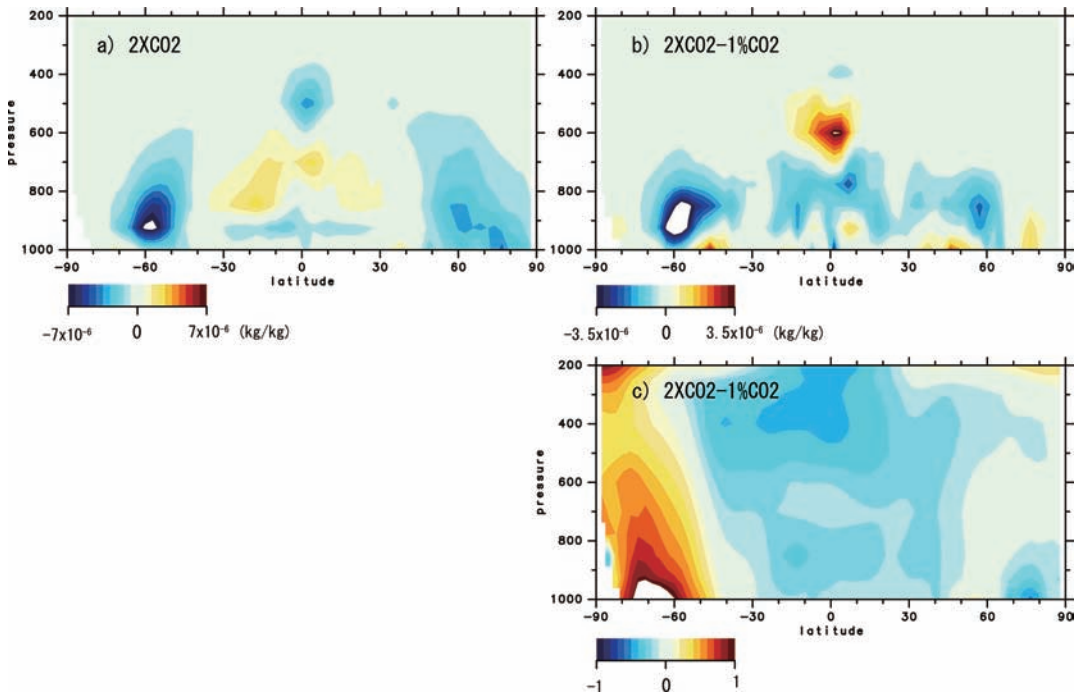

Fig. 9. The cloud water anomalies of (a) 2 × CO_2, (b) difference between 2 × CO_2 and 1%CO_2 and (c) the difference in the potential temperature anomaly between 2 × CO_2 and 1%CO_2 in MIROC-Mid. The anomalies are normalized by the globally averaged SAT anomaly. Although we only show the results of MIROC-Mid, those of MIROC-Hi shows similar feature (not shown).

Table 6. Difference in variables related to the cloud SW feedback at low latitudes between 2 × CO_2 and 1%CO_2, and uncertainty range of 1%CO_2 in the parenthesis

Model	$\Delta\gamma_{\mathrm{cld}}^{\mathrm{sw}}$	$\Delta\gamma_{\mathrm{cld}}^{\mathrm{sw}\prime}$	ΔSAT	$\Delta\theta_{\mathrm{es}}$
NCARc	0.22 (0.02)	0.23 (0.02)	0.03 (0.01)	−0.04 (4E-3)
GFDL0	−0.31 (0.03)	−0.33 (0.05)	−0.07 (0.03)	−0.06 (4E-3)
CCCma	−0.18 (0.02)	−0.14 (0.01)	−0.15 (0.02)	−0.01 (0.01)
MIROC-Hi	−0.13 (0.01)	−0.08 (0.02)	−0.07 (4E-3)	0.04 (0.01)

Note: The definitions of the variables are given in the text.

because the description of ocean and sea ice in AOGCMs is more realistic than that in ASGCMs. Our analysis indicated that $T_{2\times}$ has uncertainty concerning the problem in the experimental setting of ASGCMs. In order to reduce uncertainty in $T_{2\times}$ concerning these factors, it is important to tune the initial sea ice distributions as realistically as possible. This conclusion is consistent with Johns et al. (2006), which pointed out that the difference in initial sea ice distribution between ASGCMs and AOGCMs possibly causes the difference in ice-albedo feedback, and thus suggested that it is important to have similar sea-ice distribution in the control experiment between them.

The difference in cloud SW feedback between 2 × CO_2 and 1%CO_2 comes from both mid-to-high and low latitudes. In general, the baroclinicity anomaly of 1%CO_2 is larger than that of 2 × CO_2 due to the smaller temperature increase at high latitudes (especially at the Southern Ocean). Possibly because of this difference, the cloud SW feedback of 1%CO_2 is smaller (more negative) than 2 × CO_2 over mid-to-high latitudes in some models (INM, GFDL0, CCCma and HadGem). On the other hand, however, the cloud SW feedback of 2 × CO_2 is smaller (more negative) than 1%CO_2 over mid-to-high latitude in other models (MIROC-Mid, MIROC-Hi). This is probably caused by the larger cloud water response of 2 × CO_2 over these regions. The difference in cloud SW feedback at low latitudes is consistent with the difference in saturated stability in some models (NCARc and MIROC-Hi). However, the relationship is inverted in other models (GFDL0 and CCCma). It seems difficult to explain this only by the difference in the SAT anomaly between 2 × CO_2 and 1%CO_2 because the cloud SW feedback normalized by the local SAT anomaly is also different.

As shown in this study, the climate feedback parameter is quite different between transient and equilibrium responses. Therefore, it is reasonable to believe $\lambda_{2\times,\mathrm{eff}}$ by AOGCMs rather than $\lambda_{2\times}$ by ASGCMs when we consider the transient response of near future climate projection as performed by Harris et al. (2006). On the other hand, when we consider the equilibrium response where the CO_2 concentration is stabilized, our results support the previous results that $\lambda_{2\times,\mathrm{eff}}$ by AOGCMs approaches to $\lambda_{2\times}$ by ASGCMs (Senior and Mitchell, 2000; Watterson,

2000). This is because the largest contribution to the difference in λ between $2 \times CO_2$ and $1\%CO_2$ is the cloud SW feedback, which would depend on the difference in SAT response. As the climate system approaches equilibrium in AOGCMs, ocean temperature would increase slowly (Stouffer, 2004) and the SAT response of $1\%CO_2$ would approach that of $2 \times CO_2$.

If $\lambda_{2\times,\mathrm{eff}}$ approaches $\lambda_{2\times}$ (namely $T_{2\times,\mathrm{eff}}$ approaches $T_{2\times}$) with ocean warming, it means that the effective climate sensitivity evolves with time. From our analysis of CMIP3 climate models, we cannot tell whether the effective climate sensitivity should increase or decrease. If $T_{2\times,\mathrm{eff}}$ really approaches $T_{2\times}$, then $T_{2\times,\mathrm{eff}}$ should increase about 1.7 K in HadGem, and it should decrease about 0.8 K in MIROC-Mid and MIROC-Hi. Since the cloud SW feedback is an important factor which determines the sign and magnitude of $\Delta T_{2\times}$, investigating the cloud response should be critical to understanding how the effective climate sensitivity evolves with time.

Recently, it has been reported that part of the cloud response to CO_2 doubling in models is very rapid and should be regarded as an 'effective forcing ' which is part of the CO_2 radiative forcing component (e.g. Gregory and Webb, 2008; Williams et al., 2008). Although the effective forcing of $2 \times CO_2$ and $1\%CO_2$ has not been investigated in this study, Williams et al. (2008) report differences in the strength of the feedbacks under equilibrium condition between ASGCMs and AOGCMs, even after removing the cloud component of the effective forcing. Boer and Yu (2003) also demonstrated that the feedback strength of AOGCMs in the near equilibrium state is different from the equilibrium response of ASGCMs. The equilibrium responses from ASGCMs may not be so realistic as in AOGCMs because of their simplified sea ice and ocean physical processes. In order to understand how the climate sensitivity evolves with time, the equilibrium responses of AOGCMs require further investigation, even though this requires long integrations. Applying this analysis to equilibrium AOGCMs experiments would help to address this issue.

5. Acknowledgements

We acknowledge the international climate modelling groups, the PCMDI, and WCRP's Working Group on Coupled Modelling for their roles in making available the WCRP's CMIP3 multimodel dataset. Support of this dataset is provided by the Office of Science, U.S. Department of Energy. The authors are indebted to the IPCC Working Group One Technical Support Unit for technical support. We would like to thank the anonymous reviewers for providing valuable comments and suggestions. We gratefully acknowledge Kieth Williams, Mark Webb, Matthew Collins, and Hugo Lambert at UK Met Office for their helpful discussions. Thanks are also due to Hiroaki Kawase, Masamichi Ohba, Masahiko Ebara, Yoichi Kamae and Toshiharu Nagatomo for helping with the preparation of the model data. We also wish to thank Shaney Crawford for proofreading the manuscript. This work was supported by Innovative Program of Climate Change Projection for the 21st Century of the Ministry of Education, Sports, Culture, Science and Technology of Japan, and by the Global Environment Research Fund (S-5) of the Ministry of the Environment of Japan.

References

Boer, G. J. and Yu, B. 2003. Dynamical aspects of climate sensitivity. *Geophys. Res. Lett.* **30**, 1135, doi:10.1029/2002GL016549.

Bony, S. and Dufresne, J.-L. 2005. Marine boundary layer clouds at the heart of tropical cloud feedback uncertainties in climate models. *Geophys. Res. Lett.* **32**, L20806, doi:10.1029/2005GL023851.

Cess, R. D., Potter, G. L., Blanchet, J. P., Boer, G. L., Del Genio, A. D. and co-authors. 1990. Intercomparison and interpretation of climate feedback processes in 19 atmospheric general circulation models. *J. Geophys. Res.* **95**, 16 601–16 615.

Collins, W. D., Rasch, P. J., Boville, B. A., Hack, J. J., McCaa, J. R. and co-authors. 2004. Description of the NCAR Community Atmosphere Model (CAM3.0). Technical Note TN-464+STR, National Center for Atmospheric Research, Boulder, 214pp.

Collins, W. D., Booth, B. B. B., Harris, G. R., Murphy, J. M., Sexton, D. M. H. and co-authors. 2006. Towards quantifying uncertainty in transient climate change. *Clim. Dyn.* **27**, 127–147.

Colman, R. A. 2003. A comparison of climate feedbacks in general circulation model. *Clim. Dyn.* **20**, 865–873.

Diansky, N. A., Bagno, A. V. and Zalensny, V. B. 2002. Sigma model of global ocean circulation and its sensitivity to variations in wind stress. *Izv. Atmos. Ocean. Phys.* **38**, 477–494.

Flato, G. M. 2005. The Third Generation Coupled Global Climate Model (CGCM3). http://www.cccma.bc.ec.gc.ca/models/cgcm3.shtml.

Forster, P. M. D. and Taylor, K. E. 2006. Climate Forcings and climate sensitivities diagnosed from coupled climate model integrations. *J. Clim.* **19**, 6181–6194.

Galin, V. Ya, Volodin, E. M. and Smyshliaev, S. P. 2003. Atmospheric general circulation model of INM RAS with ozone dynamics. *Russ. Meteorol. Hydrol.* **5**, 13–22.

GFDL GAMDT (The GFDL Global Atmospheric Model Development Team) 2004. The new GFDL global atmosphere and land model AM2-LM2: evaluation with prescribed SST simulations. *J. Clim.* **17**, 4641–4673.

Gnanadesikan, A., Dixon, K. W., Barreiro, M., Beesley, J. A., Cooke, W. F. and co-authors. 2004. GFDL's CM2 global coupled climate models.Part 2: The baseline ocean simulation. *J. Clim.* **19**, 675–697.

Gregory, J. M. and Webb, M. J. 2008. Tropospheric adjustment induces a cloud component in CO_2 forcing. *J. Clim.* **21**, 58–71.

Harris, G. R., Sexton, D. M. H., Booth, B. B. B., Colllins, M., Murphy, J. M. and co-authors. 2006. Frequency distributions of transient regional climate change from perturbed physics ensembles of general circulation model simulations. *Clim. Dyn.* **27**, 357–375.

Johns, T. C., Durman, C. F., Banks, H. T., Roberts, M. J., McLaren, A. J. and co-authors. 2006. The new Hadley Center climate model (HadGEM1): evaluation of coupled simulations. *J. Clim.* **19**, 1327–1353.

K-1 model developers 2004. K-1 coupled GCM (MIROC) description. In: *K-1 Tec. Rep. 1* (eds S. Emori and H. Hasumi), Univ. of Tokyo, Tokyo, 1–34.

Kiehl, J. T., Shields, C. A., Hack, J. J. and Collins, W. D., 2006. The Climate sensitivity of the Communiti Climate System Model Version 3. *J. Clim.* **19**, 2584–2596.

Lindzen, R. S. and Farrell, B. F. 1980. A simple approximate result for maximum growth rate of baroclinic instabilities. *J. Atmos. Sci.* **37**, 1648–1654.

Martin, G. M., Dearden, C., Greeves, C., Hinton, T., Inness, P. and co-authors. 2004. Evaluation of the Atmospheric Performance of HadGAM/GEM1. Hadley Centre Technical Note No. 54, Hadley Centre for Climate Prediction and Research/Met Office, Exeter.

McFarlane, N. A., Boer, G. J., Blanchet, J.-P. and Lazare, M. 1992. The Canadian Climate Centre second-generation general circulation model and its equilibrium climate. *J. Clim.* **5**, 1013–1044.

Meehl, G. A., Covey, C., Delworth, T., Latif, M., McAvaney, B. and co-authors. 2007a. The WCRP CMIP3 multimodel dataset: A new era in climate change research. *Bull. Amer. Meteor. Soc.* **88**, 1383–1394.

Meehl, G. A., Stocker, T. F., Collins, W. D., Friedlingstein, P., Gaye, A. T. and co-authors. 2007b. Global climate projection. In: *Climate Change 2007 The physical science basis. Contribution of Working Groupe I to the Fourth Assessment Report of the Intergovernmental Panel on Climate Change* (eds S. Susan, D. Qin, M. Manning, Z. Chen, M. Marquis and co-editors), Cambridge University Press, New York, 747–845.

Murphy, J. M. 1995. Transient response of the Hadley Centre coupled ocean-atmophere model to increasing carbon dixide. Part III: analysis of global mean response using simple models. *J. Clim.* **8**, 496–514.

Ogura, T., Emori, S., Webb, M. J., Tsushima, Y., Yokohata, T. and co-authors. 2008. Towards understanding cloud response in atmospheric GCMs: the use of tendency diagnostics. *J. Meteorol. Soc. Japan* **86**, 69–79.

Pacanowski, R. C., Dixon, K. and Rosati, A. 1993. The GFDL Modular Ocean Model Users Guide, Version 1.0. GFDL Ocean Group Technical Report No. 2, Geophysical Fluid Dynamics Laboratory, Princeton.

Raper, S. C., Gregory, J. M. and Stouffer, R. J. 2002. The role of climate sensitivity and ocean heat uptake on AOGCM transient temperature response. *J. Clim.* **15**, 124–130.

Rayner, N. A., Parker, D. E., Horton, E. B., Folland, C. K., Alexander, L. V. and co-authors. 2003. Global analyses of sea surface temperature, sea ice, and night marine air temperature since the late nineteenth century. *J. Geophys. Res.* **108**, 4407, doi:10.1029/2002JD002670.

Randall, D. A., Wood, R. A., Bony, S., Colman, R., Fichefet, T. and co-authors. 2007. Climate models and their evaluation. In: *Climate Change 2007 The physical science basis. Contribution of Working Groupe I to the Fourth Assessment Report of the Intergovernmental Panel on Climate Change*, (eds S. Susan, D. Qin, M. Manning, Z. Chen, M. Marquis and co-editors), Cambridge University Press, New York, 589–662.

Rind, D. R., Hearly, C., Parkinson, C. and Martinson, D. 1995. The role of sea ice in 2 X CO_2 climate model sensitivity. Part I: the total influence of sea ice thickness and extent. *J. Clim.* **8**, 449–463.

Russel, J. L., Dixon, K. W., Gnanadesikan, A. and Stouffer, R. J. 2006. The southern hemisphere westerlies in a warming world: Propping open the door to the deep ocean. *J. Clim.* **19**, 6832–6390.

Roberts, M. J. 2004. The Ocean Component of HadGEM1. GMR Report Annex IV.D.3, Hadley Centre for Climate Prediction and Research/Met Office, Exeter.

Senior, C. A. and Mitchell, J. F. B. 1993. Carbon dioxide and climate: the impact of cloud parameterization. *J. Clim.* **6**, 393–418.

Senior, C. A. and Mitchell, J. F. B. 2000. The time-dependence of climate sensitivity. *Geophys. Res. Lett.* **27**, 2685–2688.

Shibata, K., Yoshimura, H., Oizumi, M., Hosaka, M. and Sugi, M. 1999. A simulation of troposphere, stratosphere and mesosphere with an MRI/JMA98 GCM. *Papers in Meteorology and Geophysics* **50**, 15–53.

Smith, R. D. and Gent, P. R. 2004. Reference Manual for the Parallel Ocean Program (POP), Ocean Component of the Community Climate System Model (CCSM2.0 and 3.0). Technical Report LA-UR-02-2484, Los Alamos National Laboratory, Los Alamos.

Soden, B. J. and Held, I. M. 2006. An assessment of climate feedbacks in coupled ocean-atmosphere models. *J. Clim.* **19**, 3354–3360.

Soden, B. J., Broccoli, R. S. and Helmer, R. S. 2004. On the use of cloud forcing to estimate cloud feedback. *J. Clim.* **17**, 3661–3665.

Spelman, M. J. and Manabe, S. 1984. Influence of oceanic heat transport upon the sensitivity of a model cli mate. *J. Geophys. Res.* **89**, 571–586.

Stouffer, M. J. 2004. Time scales of climate response. *J. Clim.* **17**, 209–217.

Taylor, K. E., Crucifix, M., Braconnot, P., Hewitt, C. D., Doutriaux, C. and co-authors. 2007. Estimating short-wave radiative forcing and response in climate models. *J. Clim.* **20**, 2530–2543.

Tsushima, Y., Emori, S., Ogura, T., Kimoto, M., Webb, M. J. and co-authors. 2006. Importance of th mixed-phase cloud distribution in the control climate for assessing the response of clouds to carbon dioxide increase: a multi-model study. *Clim. Dyn.* **27**, 113–126.

Watterson, I. G. 2000. Interpretation of simulated global warming using a simple model. *J. Clim.* **13**, 202–215.

Webb, M. J., Senior, C. A., Sexton, D. M. H., Ingram, W. J., Williams, K. D. and co-authors. 2006. On the contribution of local feedback mechanisms to the range of climate sensitivity in two GCM ensembles. *Clim. Dyn.* **26**, 145–165.

Wetherald, R. T. and Manabe, S. 1988. Cloud feedback processes in a general circulation model. *J. Atms. Sci.* **45**, 1397–1415.

Williams, K. and Tsedoius, J. 2007. GCM intercomparison of global cloud regimes: present-day evaluation and climate change response. *Clim. Dyn.* **26**, 145–165.

Williams, K., Ringer, M., Senior, C. A., Webb, M. J., McAvaney, B. J. and co-authors. 2006. Evaluation of a component of the cloud response to climate change in an intercomparison of climate models. *Clim. Dyn.* **26**, 145–165.

Williams, K. D., Ingram, W. J. and Gregory, J. M. 2008. Time variation of climate sensitivity in GCMs. *J. Clim.* doi:10.1175/2008JCLI2371.1.

Winton, M. 2006. Surface albedo feedback estimates for the AR4 climate models. *J. Clim.* **19**, 359–365.

Yin, J. H. 2005. A consistent poleward shift of the storm track in simulation of 21st century climate. *Geophys. Res. Lett.* **32**, L18701, doi:10.1029/2005GL023684.

Yokohata, T., Emori, S., Nozawa, T., Ogura, T., Tsushima, Y. and co-authors. 2005a. Climate response to volcanic forcing: Validation of

climate sensitivity of a coupled atmosphere–ocean general circulation model. *Geophys. Res. Lett.* **32**, L21710, doi:10.1029/2005GL023542.

Yokohata, T., Emori, S., Nozawa, T., Ogura, T., Tsushima, Y. and co-authors. 2005b. A simple scheme for climate feedback analysis. *Geophys. Res. Lett.* **32**, L19703, doi:10.1029/2005GL023673.

Yokohata, T., Emori, S., Nozawa, T., Ogura, T., Okada, N. and co-authors. 2007. Different transient climate responses of two versions of an atmosphere–ocean coupled general circulation model. *Geophys. Res. Lett.* **34**, L02707, doi:10.1029/2006GL027966.

Yukimoto, S., Noda, A., Kitoh, A., Sugi, M., Kitamura, Y. and co-authors. 2001. The new Meteorological Research Institute global ocean-atmosphere coupled GCM (MRI-CGCM2)-Model climate and variability. *Papers in Meteorology and Geophysics* **51**, 47–88.